Proceedings of the ASME 2010 3rd Joint US-European Fluids Engineering Summer Meeting and 8th International Conference on Nanochannels, Microchannels, and Minichannels
FEDSM-ICNMM2010
August 1-5, 2010, Montreal, Canada

FEDSM-ICNMM2010-30208

KOH-ETCHED NOZZLES FOR MONODISPERSE BUBBLE GENERATION IN MICROREACTORS

Philipp Lang, Stefan Bammesberger, Peter Woias
Laboratory for Design of Microsystems, Department of Microsystems Engineering – IMTEK
University of Freiburg, Georges-Köhler-Allee 102, 79110 Freiburg, Germany

ABSTRACT

Monodisperse micro bubbles are a great benefit for the direct fluorination of organic compounds, which is done via a direct injection of gaseous fluorine into the liquid reaction partner. In this two-phase system the fluorination process is improved by the large interfacial area of a chain of micro bubbles compared to slug or jet flow. A predictable generation of micro bubbles with high frequencies will lead to a higher yield and improved selectivity. Moreover, perfluorination is achievable. Here we describe the design and characterisation of a novel potassium hydroxide (KOH) etched nozzle concept for the generation of monodisperse microbubbles in a silicon microreactor. The gas is injected through the KOH-nozzle apex into a perpendicular liquid flow shearing off the gas bubbles. This concept enables a controlled variation of the bubble formation frequency and the gas-liquid interface. The control factors are the aspect ratio and the orientation of the nozzle with respect to the cross flowing liquid.

INTRODUCTION

Multiphase microchemical systems enable an increased reaction performance compared to common batch reactors [20]. Microfabricated reactors provide unique process advantages for these systems. They benefit from large interface areas and high heat and mass transfer rates due to small diffusion distances in their micro dimensions. Moreover, the mixing time is shorter and heat is removed from the reaction much more efficient as in conventional devices [5]. Beneficial use of these effects allows to run chemical reactions under much more aggressive conditions in preparative yields than in conventional reactors [2]. Moreover, new reaction pathways which are too difficult for conventional equipment can be performed in microreactors [1]. The direct fluorination of aromatics is a good example for these considerations and is already showing great potential in other research projects [18, 2, 11].

Fluorinated aromatic molecules are important as precursors in the synthesis of dyes, plant protective agents, and pharmaceuticals [3]. The presence of fluorine imparts commercially attractive properties like low surface tension, high thermal and chemical stability, and higher selectivity compared to the fluorine-free counterparts [3, 14]. Although fluorine itself is known as a fluorination agent, it is not used on a preparative synthesis scale. The direct fluorination causes difficulties due to the hazardous nature of fluorine and problems in controlling the excessive heat generation of the reaction [10]. This can lead to increased reaction rates, insufficient selectivity and, in worst case, to a runaway reaction. Hence, complex indirect methods are important in commercial use to distribute the reaction heat over several intermediate steps. However, all indirect multistep fluorination techniques like Halex and Balz-Schiemann require expensive reagents and have a low overall yield [21].

Our research aims at a new multiphase microreactor concept for a well-controlled and more efficient direct fluorination of aromatic molecules. The fluorination is run by direct injection of fluorine gas bubbles with a radius of about 90 µm into a liquid organic solvent. Since fluorine has a low solubility in commonly used organic solvents, the reaction proceeds at the gas-liquid interface, which therefore determines the fluorination process. This implies that the large interface, besides the much better heat setting, allows to handle the delicate direct fluorination process. A flexible generation of micro bubbles at high frequencies allows to regulate the effective interface area for the chemical reaction and thus the reaction rate.

The generation of gas-liquid multiphase flow in microfluidic structures has been investigated extensively in the recent years. The most outstanding structures are the micro bubble

column [9], the capillary flow focusing [6], and the T-junctions [7]. These techniques are able to generate very monodisperse bubble streams in a co-flowing liquid. However, the T-junction and the bubble collumn are restricted with their minimum size of the monodisperse bubbles to the fluid channel dimensions and generate a slug flow which is not wanted for our microreactor. Furthermore, the monodisperse bubble size of the capillary flow focusing technique is very sensitive to the volume flows of the liquid and gas phase.

To achieve independency from fluid flow and medium characteristics during monodisperse micro bubble formation a novel concept of rectangular nozzles is used. The nozzle designs have different aspect ratios with respect to the flow direction of the liquid solvent. Previous attempts with deep reactive ion etched (DRIE) nozzles show that a bubble generation using micro nozzles allows a reproducible and safe scale-up of the gas-liquid interface and, hence, a synthesis throughput with a higher selectivity [15].

Herein, we report the design, fabrication and characterisation of potassium hydroxide (KOH) etched nozzles in a silicon microreactor for the generation of monodisperse micro bubbles. The KOH etching technique allows to produce very defined rectangular nozzles at a simple and low cost fabrication method. Furthermore, it allows a better coating with an inert nickel layer which is crucial for an implementation into the fluorination reactor.

NOMENCLATUR

Bo	Bond number	—
f	bubble generating frequency	Hz
O_{bubble}	bubble surface	m^2
O_s	specific surface	m^2/m^3
r	bubble radius	m
$\dot{V}_{liquid}$	liquid flow rate	ml/h
$\dot{V}_{gas}$	gas flow rate	ml/h
We	Weber number	—

REACTOR MODEL

The reactor for the direct fluorination is a highly integrated microchemical system for multiphase reactions. This system, schematically represented in Fig. 1, consists basically of microfluidic unit operations for bubble generation, mixing, and heat dissipation. The structures are formed in micromachined silicon and protected against fluorine corrosion with a coating of electroplated nickel. This inert nickel layer is necessary because of the aggressive reaction substances fluorine and hydrogen fluoride which result from the planned reaction of toluene with fluorine gas. In principle, the gas is injected through a nozzle into a cross flowing liquid which shears off the bubbles. The induced gas phase with up to 100% fluorine generates a monodisperse bubbly flow with bubble radii of 80 µm to 100 µm, depending on

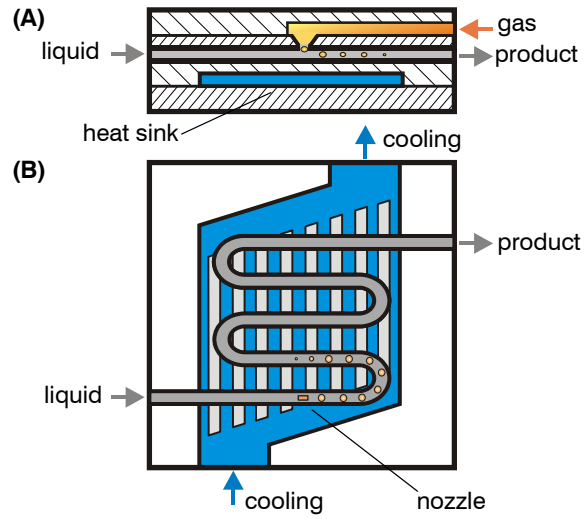

Figure 1. Schematic configuration of the microfabricated reactor. The cross-sectional view (A) shows the stacked silicon layer with the connecting layers for gas, liquid, and the heat sink. The chip has the outer dimensions of 20 mm × 20 mm, (B) top view. Both views show the unit operations of bubble generation (nozzle), mixing (meander), and heat dissipation (meander, heat sink).

the nozzles structures. While flowing through a subsequent meander channel, the two-phase flow is mixed. To enable a cooling of the highly exothermic reaction to room temperature (25°C) the heat transfer is enhanced by the same meander structures [4] and additionally by an active heat sink [8]. The volume throughput of the combined liquid-gas flow is around 100 ml/h.

The direct fluorination of aromatics is a fast gas-liquid reaction. The reaction takes place at the gas-liquid interface and depends on the diffusion of the reactants from gas phase into the liquid phase. As a result, the reaction rate is influenced by the interfacial area. The generation of smaller bubbles with higher frequencies increases the reaction rate and therefore the reaction selectivity. For that reason, the nozzle for bubble generation is the vital part of the microreactor and has been studied intensively.

NOZZLE CONCEPT FOR BUBBLE GENERATION

In this paper, we discuss the variation of different KOH etched nozzle geometries, to produce monodisperse micro bubbles with different flow rates of the liquid and gas phase. In principle, the liquid flows through a rectangular microchannel with a cross section of 300 µm × 300 µm and a length of 20 mm, as shown in Fig. 2. The gas is injected through an inverted and truncated pyramid-shaped nozzle with a height of 525 µm into the cross flowing liquid. The apex is positioned in the symmetrical center of the channel and at least 2.5 mm downstream of the fluid inlet.

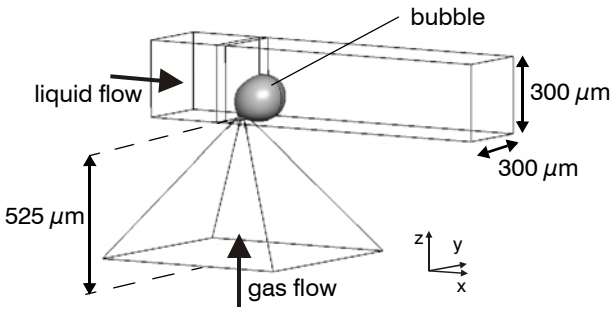

Figure 2. This picture, taken from CFD simulations, shows the configuration of the liquid channel and the obelisk shaped nozzle in one side wall. The grey shaded area depicts the gas-liquid interface of a growing gas bubble at the nozzle tip.

To analyze the influence of the aspect ratio of the nozzle tip on the generation of the micro bubbles, three different geometries were examined. The first two nozzle geometries use a geometry with a square cross section (Q: 40 μm × 40 μm) and a rectangular geometry (R1: 20 μm × 80 μm) with the same cross sectional area. A slit shaped geometry with a larger cross sectional area (S1: 20 μm × 300 μm) is used to observe the characteristics of a nozzle tip with the two smaller side walls in a virtually infinite distance from each other. To analyze the influence of the nozzle orientation with respect to the liquid flow direction the rectangular geometries are turned by 90° (R2: 80 μm × 20 μm; S2: 300 μm × 20 μm). All nozzle geometries and their orientations are depicted in Fig. 3.

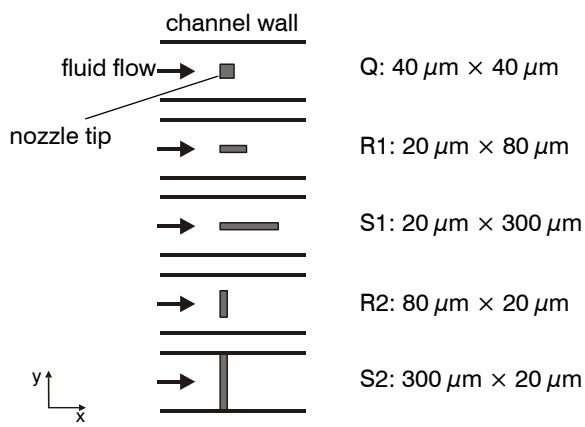

Figure 3. Top view sketch of the different nozzle tip geometries and their orientations with respect to the flow direction of the liquid channel.

DEVICE FABRICATION

The fluidic test chip was fabricated in stacked silicon and pyrex wafers. It has outer dimensions of 2 cm × 2 cm and carries three main liquid channels, each channel above one nozzle tip. These main channels have a cross section of 300 μm × 300 μm and were machined in pyrex to allow an observation of the bubble generation through the nozzle. The silicon nozzle layer is connected with a 50 μm deep gas channel fabricated in silicon layer. Figure 4 shows a picture of a complete fluidic test chip and a polished micrograph cross section through the nozzle.

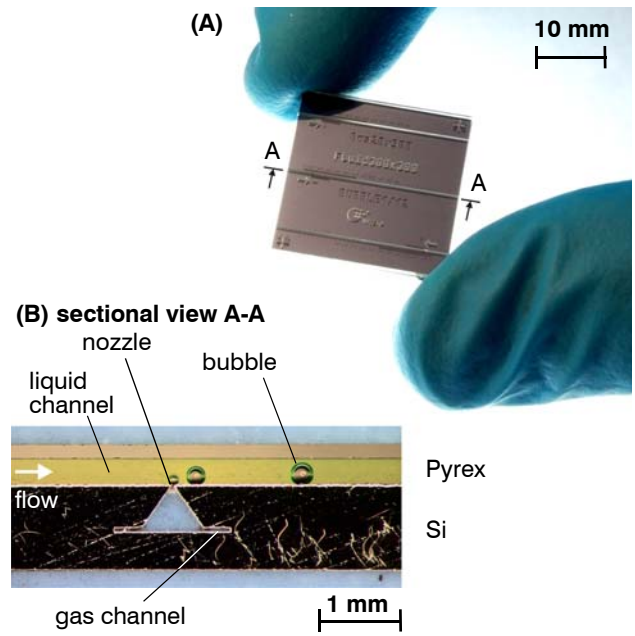

Figure 4. (A) Microfluidic test chip for bubble generation. (B) Polished micrograph section through a liquid channel with nozzle S2 (300 μm × 20 μm). The channel is filled with a fluorescein sodium solution and artificial bubbles to illustrate the bubble injection through the nozzle.

The nozzles, etched with potassium hydroxide (KOH) in <100> silicon wafers, have sloped side walls with an angle of 54.74° with respect to the plane of the wafer. This faciliates the coating with an inert nickel layer for the further use of the nozzle structure for direct fluorination. Furthermore, the KOH etching of silicon is a low-cost method and features well-defined corners and edges which are important factors for the fluidic performance of two-phase flows. The micro fabrication process to produce this test chip is schematically illustrated in Fig. 5.

A double-side polished silicon wafer (525 μm thick) is masked at front and back side with silicon oxide (SiO_2) and silicon nitride (Si_3N_4) for the KOH etch, see Fig. 5 (A). The silicon oxide was grown 300 nm thick by thermal oxidation. Over the oxide layer a 100 nm silicon nitride was deposided by low-pressure chemical vapor deposition (LPCVD). The back side of the wafer was photolitographically patterned to define the nozzles. The exposed silicon nitride/oxide was etched with reactive ion etching (RIE) to open the etch mask. Afterwards the nozzles were etched with KOH from the back side through the silicon wafer to the etch stop at the front side. This etching step fabricates a wide opening of the nozzle at the back side and a small,

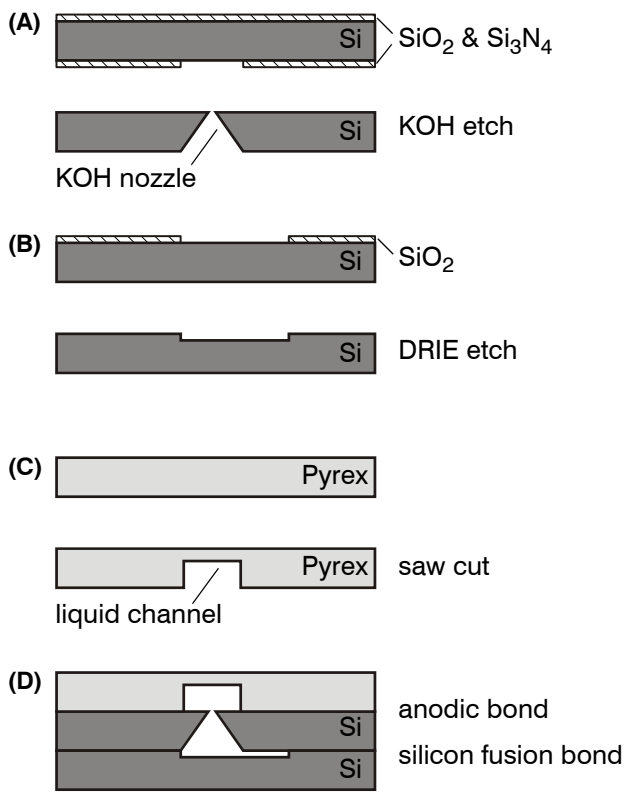

Figure 5. The fabrication process of the test chip is shown in this picture. (A) A standard silicon wafer, covered with silicon oxide (SiO_2) and silicon nitride (Si_3N_4) is etched with potassium hydroxide to fabricate the nozzle. (B) Silicon oxide covered silicon is machined with deep reactive ion etching (DRIE) to fabricate the gas supply channels. (C) The straight liquid channels in the top glass wafer are fabricated with a 300 μm wide micro saw. (D) The three layers are combined with standard MEMS bonding processes.

defined nozzle tip at the front. The silicon nitride/oxide mask was then removed by a wet chemical etching with hydrofluoric acid (HF).

Another 525 µm thick silicon wafer is covered on the top with a thermally grown silicon oxide etch mask of 1500 nm thickness, see Fig. 5 (B). A photolitographic step defines the gas channels. After opening the silicon oxide mask with RIE the gas channels were etched 50 µm deep with deep reactive ion etching (DRIE). The oxide etch mask was stripped with HF.

The main channels are machined with a 300 µm wide saw blade with a depth of 300 µm into a 500 µm thick pyrex glass wafer, see Figure 5 (C). For a highly accurate positioning of the channels the saw lines were pre-patterned with a photolithographic step.

The fabrication process of the fluidic test chip is completed by bonding the three functional layers, see Fig. 5 (D). The front of the gas channel layer is connected to the back side of the nozzle via silicon fusion bonding before the pyrex wafer is anodically bonded to the front side of the nozzle layer.

SETUP CONFIGURATION

The setup for the bubble generation experiments is shown in Fig. 6. It consists of the fluidic test chip mounted in a fluidic carrier, a syringe pump to feed the continuous liquid phase and a mass flow controller for the gas flow. The syringe pump was an *Injectomat 2000* (Fresenius, Germany) and the mass flow controller is an *El-Flow F-200CV* (Bronkhorst, Netherlands). Both were connected to the inlets of the fluidic carrier. The behavior of the bubble formation was observed through a *BX51* (Olympus, Japan) microscope with a *pco.1200* (PCO, Germany) high speed camera. The camera works with a exposure time of 150 µs which results in a frame rate of 6667 Hz for an analyzed picture frame of 610 × 142 pixels.

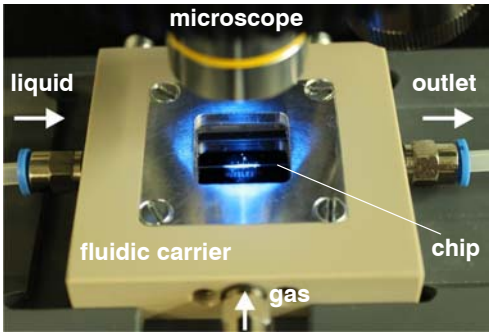

Figure 6. This picture shows the experimantal setup with the microfluidic chip mounted inside the fluidic carrier. The fluidic carrier is connected with liquid and gas supply.

Materials

To assure non-hazardous experiments we used 2-propanol as continuous phase and nitrogen gas as dispersed phase instead of toluene and fluorine gas. These substances show the same fluidic behavior for this two-phase flow system and were successfully used in prior experiments [15].

Measurements

To understand the behavior of the monodisperse bubble formation, videos were taken. The videos of the different nozzle geometries were analyzed to find the bubble generation frequency. The average of the measured frequency was calculated from three different videos taken with two minutes of delay. The frequencies had only variations between ±0.5% and ±1.7% which displays the high degree of monodispersity. The image analysis shows that the bubbles are round which correlates to simulations results of perfectly spherical bubbles [16] and they did not stick to the channel surface. This is characteristic for microfluidic systems where surface forces dominates gravitational and inertial forces, which is reflected in a small Bond and Weber number of

this system ($Bo << 1$, $We << 1$). The measurement of the bubble radii cannot be done with the needed accuracy because of the depth of focus and deep shadows of the microscope light.

With the assumption that the bubbles are spherical and no loss of gas volume flow, the bubble radius r is calculated with:

$$r = \sqrt[3]{\frac{3}{4\pi} \cdot \frac{\dot{V}_{gas}}{f}} \quad , \qquad \textbf{(1)}$$

where $\dot{V}_{gas}$ is the volumetric gas flow and f is the bubble generation frequency. The specific interface

$$O_s = \frac{f \cdot O_{bubble}}{\dot{V}_{liquid}} \qquad \textbf{(2)}$$

allows to compare the properties of generation frequency and bubble size with respect to the gas-liquid interface. The frequency f of the bubble formation and the bubble surface O_{bubble} (calculated from r) are therefore related to the volumetric flow of the liquid $\dot{V}_{liquid}$.

RESULTS AND DISCUSSION

Bubble formation frequency

We first investigated the bubble formation frequencies of the different nozzle geometries for a variation of the disperse gas flow and at three different volumetric flow rates of the constant liquid phase. This liquid flows are fixed at 50 ml/h, 75 ml/h, and 100 ml/h while the gas flow was varied between 10 ml/h and 68 ml/h. The results are illustrated in Fig. 7. The variation of the measured frequencies are smaller than 1.7% and are therefore, not shown in the graphs. All measured minimum and maximum frequencies of each nozzle represent the regime limits for monodisperse bubbly flow.

The bubble formation frequency has an effect on the gas-liquid interface which is the dominant factor for direct fluorination. A linear scaling would allow a well-controlled chemical reaction test. In our measurements we also focus to control the frequency with the size and aspect ratio of the nozzles. This enables an additional degree of freedom for the chemical reaction, independent of the flow rates from the fluids.

The measurements with a fixed liquid flow at 50 ml/h show that all nozzle geometries feature a linear increase of the bubble generation frequency with increasing gas flow, see Fig. 7 (A). The frequencies obtained with the square nozzle Q rise linear from 2142 Hz to 2759 Hz in a gas flow 19.5 ml/h and 35.5 ml/h. The rectangular nozzles show also a linear rising but nozzle R1, with the narrow side in liquid flow direction, shows higher frequencies with 2371 Hz at 19.5 ml/h gas flow and 2873 Hz at 32.5 ml/h. For example. Nozzle R2 with the wide side in flow direction shows the linear increase at lower frequencies as Q and R1, between 22.5 ml/h with 2082 Hz and 45.5 ml/h with 2782 Hz. The rectangular nozzle R1 achieves approximately 9% higher frequencies and nozzle R2 approximately 6% lower frequencies compared to the square nozzle. This means, that nozzles with equal cross sectional area generate bubbles with

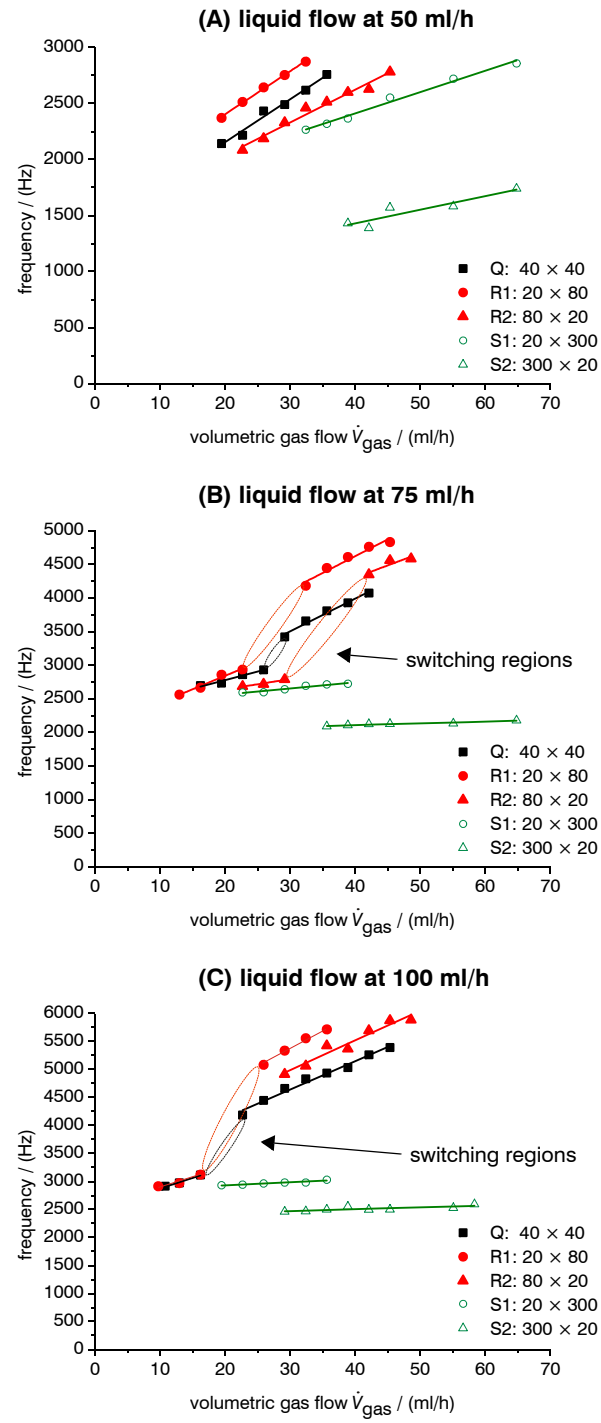

Figure 7. Comparsion of the bubble generating frequencies for all five nozzle types with a variation of the volumetric gas flow $\dot{V}_{gas}$. Graph (A) shows the generating frequencies with a fix liquid flow of 50 ml/h while (B) and (C) show them for 75 ml/h and 100ml/h liquid flow, respectively. The lines between the measured points represent the linear fit in a bubble generating regime. In (B) and (C) the regimes are divided by a frequency switching region.

different generation frequencies because of their different aspect ratio and orientation with respect to the liquid flow direction. The two slit geometries S1 and S2 have the same characteristics as the rectangular geometries (R1, R2) but at consistently lower bubble generation frequencies.

For a gas flow region between 13 ml/h and approximately 26 ml/h, the nozzles Q, R1, and R2 show, for a fixed liquid flow rate of 75 ml/h [see, Fig. 7 (B)], the same behavior as for the liquid flow of 50 ml/h [see Fig. 7 (A)]. A linear increasing bubble generation frequency is observed and nozzle R2, Q, R1 are placed in ascending order. But these bubble generating regimes ends at a volumetric gas flow of 13 ml/h for R1, 16 ml/h for Q, and 19 ml/h for nozzle R2 and change into a regime with switching frequencies. However, with a gas flow above 29 ml/h the frequencies of the three nozzles shift to a significant higher level with corresponding smaller bubble radii according to the conservation of volume. Nozzle R1 generates bubbles up to a frequency of 4831 Hz at a gas flow of 45.5 ml/h, for example. Additionally, the ascending order of the nozzles changes to Q, R2, R1. Exempted are the slit-shaped nozzles, they show a behavior similar to the experiments with a fixed flow rate of 50 ml/h.

Figure 7 (C) illustrates the measurements with a constant liquid flow rate of 100 ml/h. The nozzles Q and R1 have the same characteristics as in the measurements shown in Fig. 7 (B). A linear rise of the frequencies can be observed between 10 ml/h and approximately 16 ml/h. This bubble generation regime is followed by a region with switching frequencies between lower and higher level. Above gas flow rates of 23 ml/h a significant shift to higher bubble generating frequencies and smaller bubble radii occurs. For example, nozzle R1 produces bubbles with frequencies up to 5714 Hz at a gas flow rate of 35.5 ml/h. Furthermore, nozzle R2 starts to generate monodisperse bubbles at 30 ml/h and the highest frequency is 5883 Hz at 48.6 ml/h gas flow. Higher frequency measurements were limited by the sample rate of the high speed camera. After this shift the ascending order of the nozzles is Q, R2, R1. Once again, the slit nozzles S1 and S2 show the same characteristics as in the measurements with 50 ml/h and 75 ml/h liquid flow rate.

In general, the slit nozzles show lower bubble generating frequencies than the square and rectangular nozzles. On the other hand, they inject the bubbles with a linear increase over a large variation of gas flow without any frequency shifts and perform monodisperse bubbles at the highest gas flows compared to the other nozzles.

For all three liquid flow rates the rectangular nozzle R1 generates consistantly bubbles with higher frequencies compared to the nozzles Q and R2 with the same cross sectional area. This demonstrates that a variation of the aspect ratio, with respect to the liquid flow direction, enables a scaling of the bubble generation frequency. This effect was observed over a large variation of liquid and gas flows. Moreover, the linear performance of all nozzles gives an additional scaling factor for the chemical reactor aside from the numbering up of the nozzles in the channel.

The characteristics of the frequency-shift for the liquid flow rates of 75 ml/h and 100 ml/h suggests a limit of the bubble generating regime from lower to higher gas flow rates. We also investigated a bifurcation [17] between the two regimes with a bistable frequency of bubble generation between the lower and upper regime. A further study of these phenomena is in progress.

Generated bubble radius and specific surface

The fluid flow rates and also the shape and size of the nozzles have a big influence on bubble generation frequency and bubble radius. The average bubble size was calculated according to Eq. (1) and verified with measurements of the radius in pictures taken by the high speed camera. With increasing gas flow rate the frequencies rise linearly and the size of the bubbles expands as shown for nozzle Q ($\dot{V}_{liquid}$=50 ml/h) in Fig. 8. For this

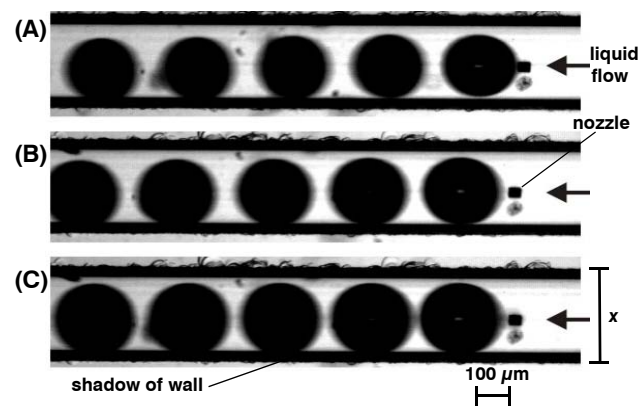

Figure 8. Sequence of the generated bubbles for nozzle Q with constant liquid flow at 50 ml/h and gas flow of (A) $\dot{V}_{gas}$ =19.5 ml/h, (B) $\dot{V}_{gas}$ =26 ml/h, and (C) $\dot{V}_{gas}$ =35.5 ml/h. The generated radii are (A) 82 *μ*m, (B) 87 *μ*m, and (C) 95 *μ*m. The channel width *x* is 300 *μ*m and the black stripes are shadows of the channel walls.

example, the radii rise from 82 μm ($\dot{V}_{gas}$=19.5 ml/h) up to 87 μm ($\dot{V}_{gas}$=26 ml/h) and 95 μm ($\dot{V}_{gas}$=35.5 ml/h). The order of the nozzle geometries in the measurements of the generation frequency (see Fig. 7) could also be observed for the radius of the injected bubbles. For instance, in the experiments with a fixed fluid flow rate of 50 ml/h [see Fig. 7 (A)] the bubble radius increases for different nozzle geometries in the same order as the bubble generating frequency, R2, Q, and R1. The bubble radii expand at a gas flow of 32.5 ml/h from 91 μm over 94 μm up to 96 μm for R2, Q, R1, respectively.

The significant shift of the bubble generating frequency at the volumetric liquid flows of 75 ml/h and 100 ml/h for some nozzle geometries are associated with a shift of the bubble radii. According to the conservation of the volume $\dot{V}_{gas}$, the radii are getting smaller for the higher frequencies [see also Eq. (1)].

For our fluorination reaction it is necessary to extend the size of the gas-liquid interface per liquid flow. The specific surface O_S [see Eq. (2)] represents this interface and summarizes the frequency and the bubble surface which is calculated from the

bubble radius. The influence of different nozzle sizes on the specific surface is shown in Fig. 9 with a fixed liquid flow rate of

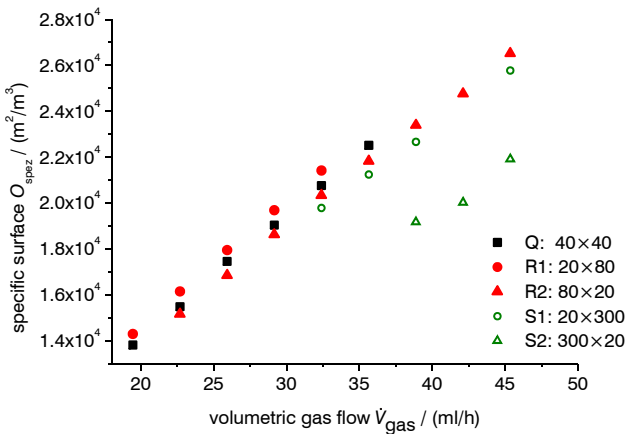

Figure 9. This graph depicts a detail of the specific surface variance at a fixed liquid flow (50 ml/h) and a increasing gas flow rate (18 ml/h to 50 ml/h).

50 ml/h and a variation of the gas flow for the square (Q) and rectangular nozzles (R1, R2). Nozzle geometry R1 creates the largest interface over the gas flow variation. The value of O_s increases linear from 14,293 m^2/m^3 at 19.5 ml/h gas flow up to 21,417 m^2/m^3 at 32.5 ml/h. The square nozzle Q shows the same linear behavior but with an approximately 3.4% smaller interface, followed by the specific interface generated by nozzle R2, which is 2.2% smaller compared to nozzle Q. The interface formed by the slit nozzle S1 is approximately 2.8% smaller as the interface of R2. Nozzle S2 is far behind, with an interface being approximately 22% smaller than the value of by nozzle R2.

These results demonstrate that it is possible to scale the interfacial area linear with an increasing gas flow, although it depends on the frequency and the bubble radius. Furthermore, a variation of the nozzle geometry with unchanged cross sectional area allows a modification of the interface, which is around 3% for the geometries Q, R1, R2. The variation between the two slit geometries is much bigger with approximately 20%.

CONCLUSION

In conclusion, we have presented a novel nozzle concept for a flexible generation of monodisperse micro bubbles which is necessary for an effective direct fluorination in a microreactor. It was possible to produce the nozzles with a low cost potassium hydroxide process, generates well-defined edges for the gas bubble injection. Moreover, the sloped side walls of the KOH nozzles facilitate a workable coating of the nozzle with an inert nickel layer for further use in the microreactor.

Measurements with varied liquid flow feature a linear scaling of the bubble generation frequency and the interfacial area with increasing gas flow. The results of the different nozzles show that the aspect ratio of the nozzle has an important role for the monodisperse generation of micro bubbles. The rectangular nozzle R1 (20 µm × 80 µm) generates the smallest bubbles with higher frequencies than the other nozzles with the same cross-sectional area. Furthermore, it was discovered that the orientation of the rectangular nozzles with respect to the liquid flow direction has a great effect on the generation frequency and the resulting interfacial area. Hence, the nozzle with the narrow side in flow direction exhibits the highest bubble formation frequency and the largest interfacial area for a wide variation of liquid and gas flows.

ACKNOWLEDGEMENT

This research was supported by the funding of the German Research Foundation (DFG). The authors appreciate the support of the Laboratory of MEMS application, IMTEK in providing of the high speed camera for the experiments.

REFERENCES

[1] Chambers, R. D., 1999, "Microreactors for elemental fluorine", Cem. Commun., pp. 883-884

[2] Chambers, R. D., Holling, D., Spink, R. C. H., Sandford, G., 2001, "Elemental fluorine – gas-liquid thin film reactors for selective direct fluorination", Lab Chip, 1, pp. 132-137

[3] Clark, J. H., Wails, D., Bastock, T. W., 1996, "Aromatic Fluorination", CRC Press, Boca Raton

[4] Dreher, S., Kronsbein, M., Woias, P., 2008, "Heat amd mass transfer and wall contact for laminar vortices in microreactors", Proc. ICNMM2008

[5] Ehrfeld, W., Hessel, V., Löwe, H., 2000: "Microreactors", Wiley-VCH, 1. Aufl., Weinheim

[6] Ganan-Calvo, A. M., Gordillo, J. M., 2001: "Perfectly Monodisperse Microbubbling by Capillary Flow Focusing", Phys. Rev. Lett. 87, 274501

[7] Garstecki, P., Fuerstman, M. J., Stone, H. A., Whitesides, G. M., 2006: "Formation of droplets and bubbles in a microfluidic T-junction—scaling and mechanism of break-up", Lab Chip, 6, pp. 437-446

[8] Haller, D., Kockmann, N., Woias P., 2009, "Simulation and experimental investigation of pressure loss and heat transfer in microchannel networks containing bends and T-junctions", Int. J. of Heat and Mass Transfer, 52, pp. 2678-2689

[9] Haverkamp, V., Hessel, V., Loewe, H., Menges, G., Warnier, M. J. F., Rebrov, E. V., de Croon, M. H. J. M., Schouten, J. C., Liauw, M. A., 2006: "Hydrodynamics and Mixer-Induced Bubble Formation in Micro Bubble Columns with Single and Multiple-Channels", Chem. Eng. Tech., 29, pp. 1015-1026

[10] Hutchington, J., Sandford, G., 1997: “Elemental Fluorine in Organic Chemistry”, Springer, Berlin/Heidelberg

[11] Jaehnisch, K., Baerns, M., Hessel, V., Ehrfeld, W., Haverkamp, V., Loewe, H., Wille, C., Guber, A., 2000, “Direct fluorination of toluene using elemental fluorine in gas/liquid microreactors”, J. of Fluorine Chem., 105, pp. 117-128

[12] Jensen, K. F., 2001, “Microreaction engineering – is smaller better?”, J. of Chem. Eng. Science, 56, pp. 293-303

[13] Kirsch, P., 2004, “Modern fluoroorganic chemistry”, Wiley-VCH, 1. Aufl., Weinheim

[14] Lagow, R. J., 1979: “Direct fluorination: A new approach to fluorine chemistry”, Prog. Inorg. Chem., 26, pp. 161-210

[15] Lang, P., Herbstritt, T., Dreher, S., Woias, P., 2010, “Nozzles for Monodisperse Bubble Generation in Microreactors”, Proc. IMRET11

[16] Lang P., Woias P., 2009: “CFD simulation and analysis of micro bubble generating nozzles for microreactors”, Proc. of Mikrosystemtechnik Kongress 2009

[17] Martien, P., Pope, S. C., Scott, P. L., Shaw, R. S., 1985, “The chaotic behaviour of the leaky faucet”, Physics Letters, 110A, pp. 399-404

[18] de Mas, N., Günther, A., Schmidt, M. A., Jensen, K. F., 2003, “Microfabricated multiphase reactors for the selective direct fluorination of aromatics”, I&EC research, 42, pp. 698-710

[19] Perry, R. H., Green, D. W., 1997, “Perry's chemical engineers' handbook”, McGraw-Hill, 7. Aufl., New York

[20] Kockmann, N., 2006: “Micro process engineering”, Wiley-VCH, 1. Aufl., Weinheim, pp. 73-113

[21] Taverner, S. J., Clark, J. H., 2003, “Can fluorine chemistry be green chemistry?”, Journal of Fluorine Chemistry, 123, pp. 31-36